Dissociation of Charge Transfer States and Carrier Separation in Bilayer Organic Solar Cells: A Time-Resolved Electroabsorption Spectroscopy Study

Andrius Devižis,*,[†,‖] Jelissa De Jonghe-Risse,[†] Roland Hany,[§] Frank Nüesch,[§,‡] Sandra Jenatsch,[§,‡] Vidmantas Gulbinas,[‖] and Jacques-E. Moser[†]

[†]Photochemical Dynamics Group, Institute of Chemical Sciences and Engineering, and [‡]Institute of Materials, École Polytechnique Fédérale de Lausanne, CH-1015 Lausanne, Switzerland

[§]Laboratory for Functional Polymers, EMPA, Swiss Federal Laboratories for Materials Science and Technology, CH-8600, Dübendorf, Switzerland

[‖]Center for Physical Sciences and Technology, Savanoriu 231, LT-02300 Vilnius, Lithuania

S *Supporting Information*

ABSTRACT: Ultrafast optical probing of the electric field by means of Stark effect in planar heterojunction cyanine dye/fullerene organic solar cells enables one to directly monitor the dynamics of free electron formation during the dissociation of interfacial charge transfer (CT) states. Motions of electrons and holes is scrutinized separately by selectively probing the Stark shift dynamics at selected wavelengths. It is shown that only charge pairs with an effective electron−hole separation distance of less than 4 nm are created during the dissociation of Frenkel excitons. Dissociation of the coulombically bound charge pairs is identified as the major rate-limiting step for charge carriers' generation. Interfacial CT states split into free charges on the time-scale of tens to hundreds of picoseconds, mainly by electron escape from the Coulomb potential over a barrier that is lowered by the electric field. The motion of holes in the small molecule donor material during the charge separation time is found to be insignificant.
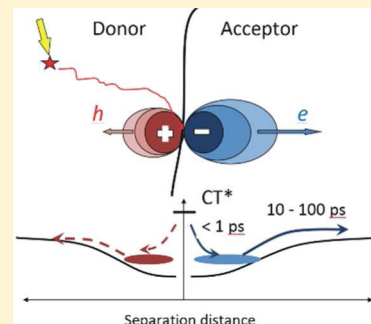
1. INTRODUCTION

Organic solar cells have recently overcome 10% efficiency[1] getting this technology closer to mass production due to lower fabrication cost as compared to conventional inorganic solar cells. Successful development of the field requires a clear understanding of all optical and electronic processes that determine the operation efficiency of organic solar cells. Surprisingly, the key operation process, that is, the photo-generation of free charge carriers, is still obscured.

Generally, charge carrier generation occurs in a sequence of several distinguishable steps: (i) photon absorption leading to creation of neutral Frenkel excitons in either the donor or acceptor material, (ii) Frenkel exciton migration to the donor/acceptor interface, (iii) charge transfer (CT) between donor and acceptor materials, (iv) formation of a coulomb bound charge pair across the heterojunction (interfacial charge transfer state), and (v) dissociation of the relaxed CT state into free charge carriers. The first three steps have been intensively investigated by means of ultrafast spectroscopy methods. It was shown that formation of the CT state from a Frenkel exciton created in the donor material is extremely fast taking place on a time scale of tens of femtoseconds.[2−7] Information about the last two processes, that is, how the CT state stabilizes and splits into free charge carriers, is more controversial. A number of studies, mainly performed in bulk heterojunction solar cells, have been published during the last several years arguing for

two different conceptions: According to the first one, charge carriers are generated from relaxed interfacial CT states and the separation is driven by carrier diffusion in disordered three-dimensional materials.[8−12] The second conception claims that charge carriers are generated on an ultrafast time scale by dissociation of hot, delocalized CT states.[13−17] Investigations have indeed demonstrated that charge pairs with electron−hole separation larger than the nearest neighbor distance are created from nonrelaxed interfacial CT states.[14,17] Ultrafast electric field optical probing techniques have been demonstrated as a very useful tool for the investigation of electrical charge separation and transport phenomena in organic semiconductors.[15,18−20] These experimental approaches employ electric field-dependent optical response of the investigated material, be it field-induced second harmonic generation or Stark effect. Photogeneration of the charge pairs, splitting of these pairs, and subsequent carrier drift result in the modification of macroscopic and/or microscopic distributions of the electric field in the material, causing modifications in its optical properties. Tracking the temporal evolution of these properties in the optical pump−probe scheme enables the reconstruction of the electric field and, hence, the dynamics of charge motion. Gélinas et al.[15] evaluated from analysis of the Stark shift input into the

transient absorption signal that charge carriers are separated by at least 4 nm by electron delocalization and coherent propagation inside fullerene domains. The authors considered that the remaining coulomb attraction barrier is low so that charge carriers created after this ultrafast propagation may be considered as free. However, experimentally, the subsequent charge pair evolution remained undisclosed. The ~4 nm separation distance of the electron−hole pair is much shorter than the coulomb capture radius, estimated to be about 12−15 nm. We have also investigated the carrier drift dynamics in bulk heterojunction solar cells by means of the ultrafast optical probing of the electric field kinetics.[21] These measurements revealed ultrafast evolution of the average carrier drift distance. The charge pair separation dynamics in these measurements, however, was convoluted with the complex three-dimensional motion of already separated charge carriers in the disordered bulk heterojunction. Formation of interfacial charge transfer states and their dissociation into free charge carriers in planar heterojunction solar cells were more rarely addressed. These processes are expected to be governed by the same physical interactions and material properties as in bulk heterojunction solar cells. Because of precisely known geometrical parameters and a well-defined geometrical plane where separation of the charges takes place, CT state dynamics and free carrier separation in bilayer solar cells are expected to be less entangled. The averaged microscopic displacement of charges at the planar heterojunction results in macroscopic perturbation of the electric field in the donor and in the acceptor layers. In addition, transport of photogenerated electrons and holes is spatially separated. Thus, planar heterojunction solar cells may serve as an ideal model system for the investigation of the charge carrier generation phenomenon.

To the best of our knowledge, the carrier escape from the Coulomb attraction and the dynamics leading to free charge carriers have not been addressed explicitly so far, probably because of the absence of appropriate experimental methods capable to disclose the carrier motion within organic photovoltaic devices with a sufficient time resolution. Here we investigate the free charge carrier formation process by use of ultrafast time-resolved Stark effect spectroscopy, which allows one to probe directly the electric field dynamics in cyanine/fullerene bilayer solar cells. The important advantage of the Stark effect technique when applied to planar heterojunction solar cells is that it allows one to distinguish between the electron and hole motions by analyzing different spectral regions, as long as electroabsorption (EA) of the donor and acceptor materials is spectrally separated. Moreover, fast CT state formation, fast electron motion in thin fullerene layer, and close to one-directional carrier motion enabled us to distinguish between CT state formation, coulomb bound charge pair separation, and carrier drift processes. We demonstrate that charge pairs with an effective separation distance of less than 4 nm are created on an ultrafast time scale at the small molecule/fullerene interface, while dissociation of coulomb bound charge pairs into free charge carriers takes place on the tens to hundreds of picoseconds time scale from the relaxed CT state mainly by the electron motion.

2. EXPERIMENTAL SECTION

OPV cells with planar heterojunction architecture were prepared by spin-coating a solution in 2,2,3,3-tetrafluoropropanol of the trimethine cyanine dye Cy3 with PF_6^- as a counterion (Cy3-P) and by vacuum thermal evaporation of C_{60} on top of the dye layer. The molecular

structures of the investigated materials and their energy levels are shown in Figure 1. A detailed sample preparation method has been
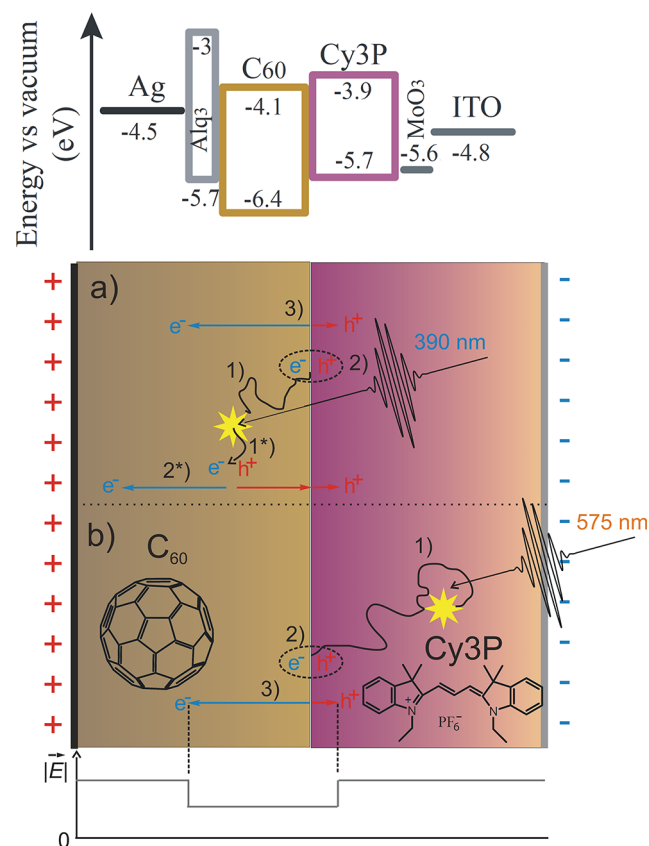

Figure 1. Energy level diagram of the solar cell (upper scheme). Schematic illustration of charge formation in a C_{60}/Cy3-P planar heterojunction solar cell and the resulting redistribution of the electric field under pulsed excitation conditions (bottom scheme): (1) diffusion of the photogenerated exciton toward the interface; (2) formation and splitting of the interfacial CT state; (3) drift of free charge carriers. Processes marked by an asterisk refer to electric field-assisted generation (1*) and drift (2*) of free charges in the bulk of C_{60}. Part (a) represents the case of acceptor excitation (390 nm), and part (b) donor excitation (575 nm).

reported elsewhere.[22] Such cyanine dye/fullerene bilayer organic solar cells have shown lately up to 3.2% power conversion efficiency, with a short-circuit current J_{sc} = 6.5 mA·cm^{-2}, an open-circuit voltage V_{oc} = 0.95 V, and a fill factor FF = 52.4%.[23] The thorough analysis of the device performance can be found in ref 24.

The experimental setup used for the electromodulated differential absorption (EDA) measurements was implemented on a conventional femtosecond absorption pump−probe spectrometer. More details can be found in ref 25.

3. RESULTS AND DISCUSSION

The time-resolved Stark effect technique consists in probing the dynamics of spectral shifts in the transient absorption of a bilayer sample submitted to an external static electric field. Excitons created by a light pulse in the bulk of the cyanine Cy3-P layer diffuse and are quenched at the donor−acceptor interface by electron transfer from the Cy3-P to the energetically lower lying LUMO of C_{60}. Diffusion of the excitons does not affect the electric field felt by the donor material, but the electric field distribution starts being affected as electrons are injected into the acceptor layer and CT states

are created at the interface. The effect is twofold: First, local electric fields appear with the electron injection into the acceptor layer. Second, dissociation of the CT states is followed by the drift of the formed free charge carriers toward the corresponding electrodes, and this reduces the macroscopic built-in or applied electric field. The extraction of electrons and holes reduces the field in the acceptor and donor layers, respectively (see Figure 1). The analogy may be applied for the case of acceptor excitation, except that exciton diffusion takes place in the acceptor layer and a hole is injected into the HOMO of the donor at the interface. As we show below, field-assisted free charge generation in the bulk of the electron acceptor C_{60} may also significantly contribute to photocurrent if an external bias is applied to the device.

The application of this technique is based on the measurement and analysis of the time-resolved EDA spectra. The EDA is an optical pump−probe method designed to measure the absorption difference between a biased and unbiased sample as a function of probe delay. General aspects of the EDA technique were discussed in the literature.[18,20]

The steady-state EA spectra of pristine Cy3-P, pristine C_{60} and C_{60}/Cy3-P (30/20) bilayer devices measured under an applied reverse bias are presented in Figure 2. Here and further

presence of the electric field.[27,28] A red band at 585 nm and a blue band at 445 nm are observed in the spectra of pristine Cy3-P. Importantly, there are regions in the visible spectrum where the EA bands of C_{60} and Cy3-P are not overlapping. For instance, the EA amplitude of Cy3-P is zero in the range from 500 to 550 nm, exactly where EA of C_{60} is the strongest. The red band of Cy3-P at 585 nm overlaps only slightly with the red tail of the C_{60} main peak. Spectral separation of the Cy3-P and C_{60} EA allows independent monitoring of changes of the electric field in each of the layers by analyzing different spectral regions in time-resolved EDA experiments. In addition, selective excitation of the donor or acceptor layer is also possible by appropriate choice of the excitation wavelength. The absorbance maximum of Cy3-P is located at 575 nm, where the absorbance of C_{60} is weak. The opposite situation prevails in the near-UV where Cy3-P does not absorb, while C_{60} has a rather strong absorbance (Figure 2).

The steady-state amplitude of C_{60} EA peaks at 540 and 505 nm scale quadratically with the applied bias (inset of Figure 3a). Photoexcitation of the device, as it was discussed, causes reduction of the electric field and weakening of the EA amplitude. Electrons drifting away from the interface in the C_{60}
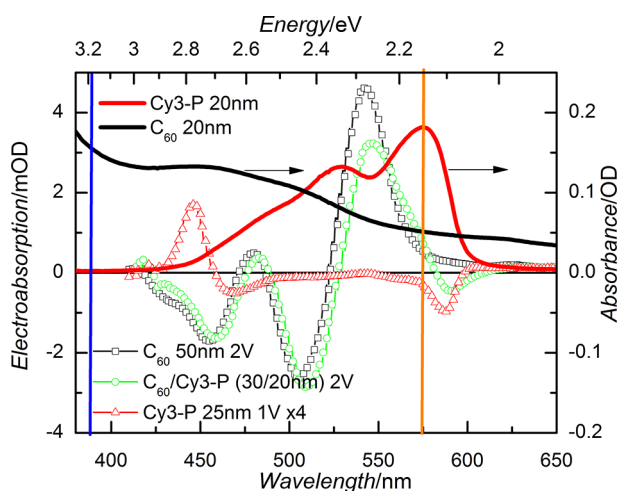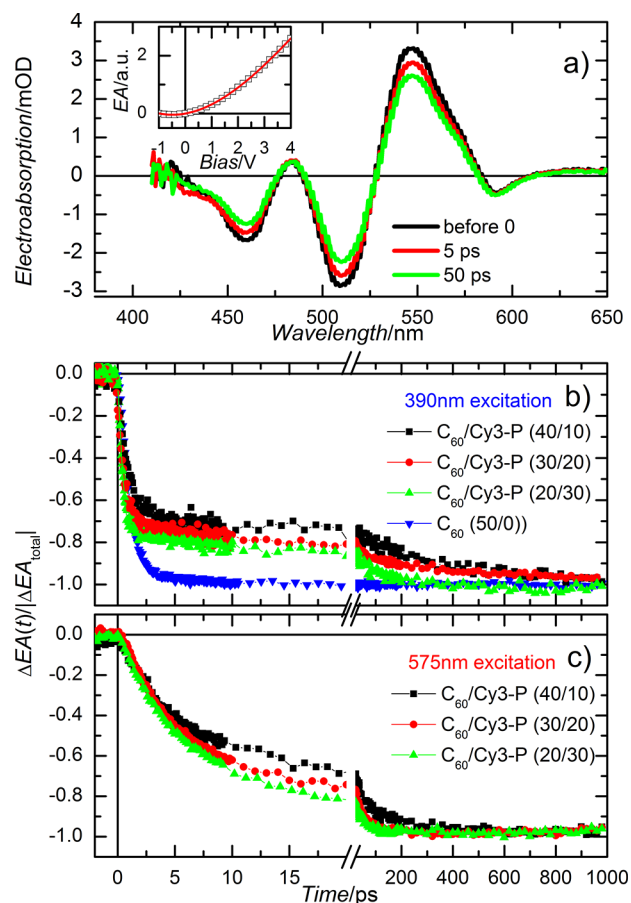

Figure 2. Electroabsorption spectra of pristine C_{60}, pristine Cy3-P films, and C_{60}/Cy3-P bilayer devices (data points, bias voltages, and thicknesses as indicated in the label). Absorption spectra of pristine films are also shown (right scale, full lines). Vertical lines show both 390 and 575 nm wavelength excitation chosen for selective excitation of C_{60} and Cy3-P, respectively.

in the text the label C_{60}/Cy3-P (−/−) denotes the thickness of the corresponding layers of the device. In this case (30/20) means that the thickness of the C_{60} layer is 30 nm and the thickness of the Cy3-P layer is 20 nm. Dark currents under reverse bias were negligible (below 1 mA/cm^2) and, thus, charge concentration in the active layers was virtually zero. This situation results in a homogeneously distributed electric field for different layer thicknesses and in both layers of the bilayer structure. The EA spectrum of C_{60} displays two main features: a positive peak located at 540 nm and a negative one at 505 nm. This spectrum is consistent with the one reported in literature.[26,27] Notably, the EA spectrum doesn't follow the first or the second derivative of the absorption spectrum. This is due to the forbidden optical transition from A_g ground state to H_g symmetry excited state that becomes allowed in the

Figure 3. (a) EDA spectra of a C_{60}/Cy3-P (30/20) device at different time delays after 575 nm excitation, 0.2 μJ/cm^2, for 4 V applied bias. The inset shows the steady-state dependence of the EA amplitude on the applied bias. Electroabsorption dynamics in the C_{60} layer of planar heterojunction devices of different compositions at (b) 390 nm (0.7 μJ/cm^2) and (c) 575 nm excitation wavelength (0.2 μJ/cm^2) with 2 V applied bias (∼0.5 MV/cm). Part (b) includes the electric field dynamics in a pristine C_{60} film.

layer and geminate holes create electrical dipoles, which counteract the initial electric field (Figure 1). All measurements were performed at small charge drift conditions;[29] that is, the excitation intensity was chosen in a way that the concentration of photogenerated carriers was too low to perturb the initial electric field significantly. Thus, the excitation-induced variation of the field was small in comparison to the applied field, and the motion of charges might be considered as taking place in a quasi-static electric field. Figure 3a shows the EDA spectra of the bilayer device C_{60}/Cy3-P (30/20) at different delay times after excitation by a laser pulse at 575 nm wavelength. In general, EDA data may also include the absorption changes caused by field-affected population of the excited state(s). This contribution was negligible at the low excitation energy fluence of 0.2 $\mu J/cm^2$ (Figure 3a), as no shift of the spectral bands or appearance of new band is observed. Moreover, only the C_{60} EA bands experience a decay in time, while the EA band at 585 nm attributed to Cy3-P remains constant during the optically probed time interval of 1 ns. Thus, the major contributor to the EDA dynamics is the decaying electric field in the C_{60} layer related to the drift of photogenerated electrons. Apparently, the holes' drift in Cy3-P is much slower. This is in agreement with the low hole mobility of about 10^{-5}–10^{-7} $cm^2/(V{\cdot}s)$ in Cy3-P[22] with respect to the electron mobility of the order of 1 $cm^2/(V{\cdot}s)$ in C_{60}.[30−33] Accordingly, we expect hole motion on a microsecond time scale that is confirmed by integral mode time-of-flight data (see the Supporting Information (SI)).

Figure 3b (acceptor excitation) and Figure 3c (donor excitation) show the dynamics of the EA absolute amplitude integrated in the spectral region between 500 and 560 nm, where the main peak of the C_{60} electroabsorption is located. The EA changes are normalized to the total EA change (ΔEA_{total}) calculated from the time-integrated photocurrent measured with the oscilloscope. The time-integrated photocurrent divided by the sample capacitance yields the total reduction of the electric field (voltage). In conjunction with the steady-state dependence of the EA versus bias, this enables one to estimate ΔEA_{total}, the change of EA when all electrons are extracted from bilayer devices or all charges from the single C_{60} layer device. Thus, reaching the "−1" level indicates that all electrons (or all electrons and holes in the case of single C_{60} layer) were extracted from the sample—a plateau extending to 1 ns as determined from optical measurements corresponds to the same level as obtained at long times from time-integrated electrical measurements of the photocurrent which is not able to resolve the picosecond dynamics due to its limited time-resolution. The obtained electric field dynamics are qualitatively similar for different device compositions, but strongly differ depending on the selective excitation of the C_{60} (390 nm, Figure 3b) or Cy3-P (575 nm, Figure 3c) layer.

First, we discuss results for the neat C_{60} device (390 nm excitation, blue curve in Figure 3b). The amount of extracted charges increases almost linearly with applied bias (see the SI) for this sample. This indicates field-assisted generation of free carriers in the bulk of C_{60}. Quite efficient carrier generation in C_{60} is related to the existence of CT states (within C_{60}, not to be confused with CT states at the interface) located at higher energies than Frenkel exciton states.[34] Thus, carrier generation in the bulk of C_{60} is expected to be very fast taking place before relaxation to the Frenkel exciton state. We observe a very fast decay of the EA in this sample. During the first few picoseconds, final reduction of the EA is reached. This confirms ultrafast carrier generation and indicates that carrier extraction

is also very fast. Notably, we expect both, electrons and holes, to drift and be extracted on the same fast time-scale. Decay of the EA in pristine C_{60} film within a few picoseconds is consistent with mobilities of the order of 1 $cm^2/(V{\cdot}s)$ for both types of carriers.[30,31] Thus, free carriers are extracted from the C_{60} film on the time-scale from few to several picoseconds at a field strength of about 0.5 MV/cm.

Very similar EA dynamics were also observed in bilayer devices (Figure 3b) when C_{60} was selectively excited at 390 nm. One can notice that the initial decay is slightly faster for the devices with thinner C_{60} layer. This is a consistent observation as the extraction of the charge carriers is faster from the thinner film. The main difference between the pristine C_{60} and bilayer devices is the appearance of a slow component in the EA decay, which constitutes about 20−25% of the total amplitude in bilayers. We suggest that the fast component corresponds to the same field-assisted mechanism of free charge generation from CT states in the bulk of the C_{60} layer as in the pristine C_{60} device, while the slow component is attributed to the diffusion of Frenkel excitons in the C_{60} layer followed by charge generation at the interface between C_{60} and Cy3-P. This slow decay is consistent with the relatively slow exciton diffusion in C_{60}[35] and the exciton lifetime of about 1.2 ns.[36−38] Contribution of the fast decay component, which is attributed to field-assisted charge generation, is slightly larger for the devices with thinner fullerene layer. This is explained by the redistribution of the applied field in the bilayer according to relative permittivity of each of the layers. The cyanine has by about a factor of 1.5 higher relative permittivity than the fullerene. At the same applied voltage and the same overall thickness of 50 nm, the electric field in the fullerene layer is stronger for those devices where this layer is thinner.

The rate of the EA decay in the C_{60} layer is slower if Cy3-P is excited (Figure 3c). In this case, free electrons in fullerene are generated only by dissociation of interfacial CT states created after Frenkel excitons in Cy3-P diffusionally reach the interface. The EA decay rate is determined by exciton diffusion to the interface, formation of the interfacial CT states, their splitting into pairs of free charge carriers and electron drift through the C_{60} layer. There are several indications that exciton diffusion in Cy3-P is not a major retarding factor. First, the decay of the electric field is virtually independent of the Cy3-P layer thickness: the diffusion time is expected to be proportional to the square of the distance, and therefore, one would expect a strong dependence. Surprisingly, the opposite was observed: the decay is the slowest in the C_{60}/Cy3-P (40/10) device having the thinnest Cy3-P layer. Second, our ultrafast fluorescence measurements revealed a Cy3-P exciton lifetime in the planar heterojunction devices of the order of a few picoseconds (see the SI), indicating very fast exciton diffusion and quenching at the interface with C_{60}, that is, much shorter than the carrier extraction. And third, the rate of the EA decay increases with applied bias (see Figure 4). Diffusion of excitons, which are neutral particles, cannot be influenced by the field. The second process, CT exciton formation, was determined to take place on a femtosecond time scale in different bulk heterojunction solar cells. Moreover the fast fluorescence decay also limits this time to several ps at most. Electron extraction rate also cannot be the main retarding factor, because this time, for the applied voltages of 1−4 V, it remains on a few picosecond time scale, according to the result at 390 nm excitation (see the SI).
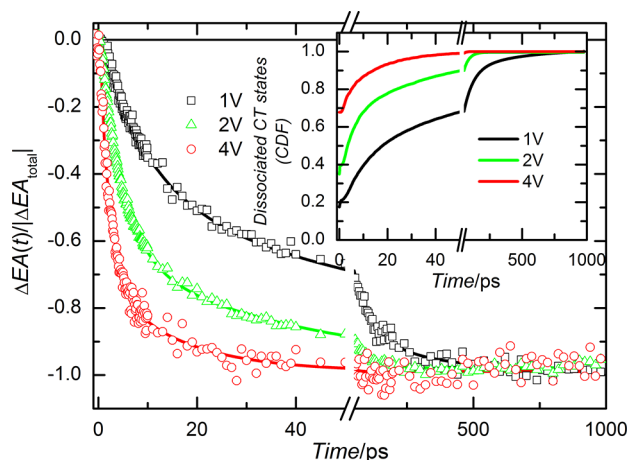
Figure 4. Electroabsorption dynamics in the C_{60} layer of the C_{60}/Cy3-P (30/20) device at 575 nm excitation wavelength (0.2 μJ/cm^2) and different applied biases. Data points indicate experimental data, and lines are results from modeling. The inset shows obtained cumulative distribution functions (CDF) of the CT state lifetime (t_{ct}) at the corresponding biases.

These considerations lead to the conclusion that dissociation of the interfacial CT state into free charge carriers is the major rate-limiting process. Its rate depends on the applied electric field, which, apparently, lowers the energy barrier for free charge formation created by intrinsic attraction of geminate countercharges. The time scale of the decay lies in the range of tens of picoseconds, indicating that a relaxed CT state is the major precursor to free charge carriers, while contribution of vibrationally "hot" CT states to the formation of free charge carriers is minor.

The relatively slow, field-stimulated EA decay in our data implies that the electron for some time remains in the potential well once it is injected from Cy3-P into the fullerene layer. We have no information if the charge carriers during this time are localized on the nearest neighbor Cy3-P and fullerene molecules (CT state), or are separated by larger distances and delocalized to some extent in donor or acceptor domains. We refer to this state as an interfacial CT state, although, "geminate charge pair" may be a synonym.

We can set an upper limit for the effective charge separation distance in the CT state from the analysis of the EA kinetics at different applied voltages. Generally, it would be possible to reconstruct the exact motion kinetics of electrons according to the EA dynamics, but there is fundamental uncertainty at close electron−hole separation distance, were the point-charge approximation fails. Gélinas et al. considered EA as originating from the local electric fields that appear as the charges climb the potential well of Coulomb attraction, separate and gain potential energy in the form of electrostatic field.[15] Notably, we did not observe any increase of EA in the bilayer and in the pristine C_{60} samples. Also, there was no detectable signal in the zero-field transient-absorption data at the given fluence of 0.2 μJ/cm^2 (not shown), which would indicate electroabsorption originating from the local fields of CT states. Thus, we conclude that the electroabsorption caused by the CT states was negligible in comparison with the electroabsorption decay caused by drifting electrons. The monitored EA signal is proportional to the square of the electric field integrated over the probed volume (EA $\sim \int E^2 dV$). The electric field energy is also proportional to the same integral. Therefore, the change of

EA induced by the motion of the carrier is determined by the potential in which it is moving. This potential greatly depends on the delocalization of the charges and delocalization is named among the key factors that facilitate charge separation. Figure 5
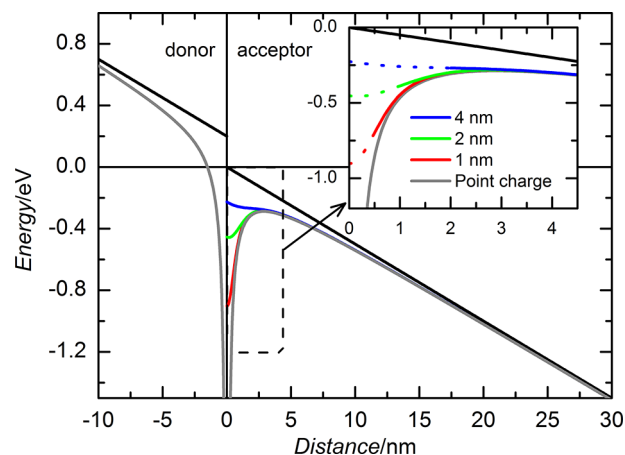

Figure 5. Hypothetic electron potential in the bilayer device at the electric field of 0.5 MV/cm (black lines). The dielectric constant of the media is 3.61[40] and the zero energy is assigned to the electron at the interface without counter charge. The curves show potentials in the presence of a positive point charge at the interface and different electron delocalization, from point charge to Gaussian width of 4 nm (width at 1/e of the maximum amplitude).

shows calculated electron potentials for an electric field of 0.5 MV/cm in the vicinity of a positive point charge for different electron delocalization degrees. The potentials of delocalized electrons were calculated assuming Gaussian distribution of the electron density. The potential profiles for three different Gaussian widths of 1, 2, and 4 nm are presented. It follows that the upper limit for the delocalization is of about 4 nm, because the barrier disappears at this delocalization dimension at the applied electric field of 0.5 MV/cm (corresponds to 2 V of applied bias in our experiments). The fact that we do not observe any increase of the EA does not contradict the existence of the potential barrier. More likely, electrons do not stay on the potential slope for a long time. They either fall back to the close CT state (bottom of the potential well) or drift toward the electrode. As a result, the number of the electrons which may give an increase of the EA is always lower than the number of already extracted electrons, which reduce the EA. We have exploited this assumption in the modeling of CT state dissociation dynamics.

The exciton diffusion in Cy3-P and electron motion through the C_{60} layer are faster than the CT state dissociation, but nevertheless, they also contribute to the delayed EA decay. Since all three processes overlap in time, the initial decay of EA is a result of the entanglement of the exciton quenching determined by the exciton diffusion, the CT state dissociation and the electron drift. In order to disentangle these processes and to get information about the CT dissociation dynamics, we have modeled the EA kinetics relying on the available information about the exciton quenching dynamics and drift of free electrons. The model accounted for the statistically distributed CT state formation and dissociation times as well as for electron drift duration through the C_{60} layer. The latter was evaluated from the electroabsorption dynamics for C_{60} excitation as described above. The dynamics of CT state

formation was obtained from the fluorescence decay kinetics assuming that quenching of Frenkel exciton instantaneously leads to creation of the CT state. Thus, the distribution of CT state life (dissociation) times was a single free parameter, which we obtained from the best fit of experimental and calculated electroabsorption kinetics (see the SI for more details).

The modeled electroabsorption decay is shown in Figure 4 by solid lines. The inset presents the obtained cumulative distribution function (CDF) of CT state lifetimes. If all CT states were created simultaneously, CDF could be considered as a relative number of dissociated CT states versus time. In reality, the concentration of CT states evolves a bit differently because the formation of the CT states is spread because of the finite duration of the initiating pump pulse and, mainly, because of the exciton diffusion. Clearly, as follows from the inset of Figure 4, the applied bias enhances the rate of CT dissociation. Only a small fraction of about 20% of CT states dissociate rapidly on the sub-picosecond time scale. The rest dissociate much slower, up to 100 ps and later at the applied bias of 1 V. Clearly nonexponential dissociation of the CT states reflects the intrinsic disorder of the system. The number of instantaneously dissociating CT states increases to about 40% and 70% at 2 and 4 V of applied bias, respectively. We relate this to the elimination of the potential barrier for electron–hole separation by the applied electric field. This experimental method cannot track the CT dissociation at low electric fields because of the limited sensitivity, but, following the observed trend, prompt dissociation is likely absent and retarded dissociation is slow at the operation conditions of the Cy3-P bilayer solar cell. The CT states existing up to hundreds of picoseconds must be quasi-equilibrated at the given temperature and electric field, thus losing the memory of initial conditions of electron injection to the acceptor layer. The conclusion is that the initial separation is not a determining factor for the splitting of the CT states. This conclusion is supported by efficient charge separation by relaxed CT states at organic interfaces demonstrated in ref 39.

4. CONCLUSION

In conclusion, spectral separation of electroabsorption bands of electron donating material Cy3-P and accepting C_{60} enabled independent monitoring of electric field dynamics in each material of planar heterojunction organic solar cell by means of ultrafast transient Stark shift spectroscopy. Electron and hole motion dynamics during their separation at the donor/acceptor interface and drift through the corresponding material were identified from the perturbation of the electric field by photogenerated charge carriers. Our results revealed very fast electron drift within C_{60} with mobility of the order of 1 cm^2/ (V·s) and much slower (by 5 orders of magnitude) hole drift within Cy3-P, implying that electron motion is responsible for the carrier separation. Modeling of the electroabsorption dynamics led to the conclusion that, after creation of the CT state, electrons delocalize in fullerene domains no more than 4 nm and their complete escape from the coulomb potential created by holes remaining at close proximity to the interface takes hundreds of picoseconds at electric fields typical for solar cell operation conditions. Thus, we show that the electron escape from the Coulomb potential is a rate-limiting process for free carrier generation and rule out "hot" CT states as a dominating pathway for charge separation. We believe that dynamics and mechanism of charge separation are qualitatively similar at donor/acceptor interfaces of bulk heterojunction

small molecule/fullerene solar cells. Consequently, for efficient solar cell performance, the electron accepting material shall ensure efficient electron delocalization and its unperturbed motion at distances beyond the coulomb potential well.

■ ASSOCIATED CONTENT

ⓈSupporting Information

Reverse bias effect on photocurrent, fluorescence, modeling of the electric field dynamics with CT state lifetime, and integral mode time-of-flight measurement. The Supporting Information is available free of charge on the ACS Publications website at DOI: 10.1021/jacs.5b03682.

■ AUTHOR INFORMATION

Corresponding Author

*devigy@ar.fi.lt

Notes

The authors declare no competing financial interest.

■ ACKNOWLEDGMENTS

■ REFERENCES

(1) Green, M. A.; Emery, K.; Hishikawa, Y.; Warta, W.; Dunlop, E. D. *Prog. Photovoltaics: Res. Appl.* **2014**, *22*, 701−710.

(2) Barbour, L. W.; Hegadorn, M.; Asbury, J. B. J. *J. Am. Chem. Soc.* **2007**, *129*, 15884−15894.

(3) Parkinson, P.; Lloyd-Hughes, J.; Johnston, M. B.; Herz, L. M. *Phys. Rev. B* **2008**, *78*, 115321.

(4) Hwang, I.-W.; Moses, D.; Heeger, A. J. *J. Phys. Chem. C* **2008**, *112*, 4350−4354.

(5) Piris, J.; Dykstra, T. E.; Bakulin, A. A.; van Loosdrecht, P. H. M.; Knulst, W.; Trinh, M. T.; Schins, J. M.; Siebbeles, L. D. A. *J. Phys. Chem. C* **2009**, *113*, 14500−14506.

(6) Marsh, R. A.; Hodgkiss, J. M.; Albert-Seifried, S.; Friend, R. H. *Nano Lett.* **2010**, *10*, 923−930.

(7) Cook, S.; Katoh, R.; Furube, A. *J. Phys. Chem. C* **2009**, *113*, 2547−2552.

(8) Blom, P. W. M.; Mihailetchi, V. D.; Koster, L. J. A.; Markov, D. E. *Adv. Mater.* **2007**, *19*, 1551−1566.

(9) Lee, J.; Vandewal, K.; Yost, S. R.; Bahlke, M. E.; Goris, L.; Baldo, M. A.; Manca, J. V.; Voorhis, T. V. *J. Am. Chem. Soc.* **2010**, *132*, 11878−11880.

(10) Vithanage, D. A.; Devižis, A.; Abramavičius, V.; Infahsaeng, Y.; Abramavičius, D.; MacKenzie, R. C. I.; Keivanidis, P. E.; Yartsev, A.; Hertel, D.; Nelson, J.; Sundström, V.; Gulbinas, V. *Nat. Commun.* **2013**, *4*, 2334.

(11) Albrecht, S.; Vandewal, K.; Tumbleston, J. R.; Fischer, F. S.; Douglas, J. D.; Fréchet, J. M.; Ludwigs, S.; Ade, H.; Salleo, A.; Neher, D. *Adv. Mater.* **2014**, *26*, 2533−2539.

(12) Jailaubekov, A. E.; Willard, A. P.; Tritsch, J. R.; Chan, W. L.; Sai, N.; Gearba, R.; Kaake, L. G.; Williams, K. J.; Leung, K.; Rossky, P. J.; Zhu, X. Y. *Nat. Mater.* **2013**, *12*, 66.

(13) Gregg, B. A. *J. Phys. Chem. Lett.* **2011**, *2*, 3013−3015.

(14) Bakulin, A. A.; Rao, A.; Pavelyev, V. G.; van Loosdrecht, P. H.; Pshenichnikov, M. S.; Niedzialek, D.; Cornil, J.; Beljonne, D.; Friend, R. H. *Science* **2012**, *335*, 1340−1344.

(15) Gélinas, S.; Rao, A.; Kumar, A.; Smith, S. L.; Chin, A. W.; Clark, J.; van der Poll, T. S.; Bazan, G. C.; Friend, R. H. *Science* **2014**, *343*, 512−516.

(16) Deibel, C.; Strobel, T.; Dyakonov, V. *Phys. Rev. Lett.* **2009**, *103*, 036402.

(17) Grancini, G.; Maiuri, M.; Fazzi, D.; Petrozza, A.; Egelhaaf, H. J.; Brida, D.; Cerullo, G.; Lanzani, G. *Nat. Mater.* **2013**, *12*, 29−33.

(18) Gulbinas, V.; Kananavičius, R.; Valkunas, L.; Bässler, H. *Phys. Rev. B* **2002**, *66*, 233203.

(19) Devižis, A.; Serbenta, A.; Meerholz, K.; Hertel, D.; Gulbinas, V. *Phys. Rev. Lett.* **2009**, *103*, 027404.

(20) Cabanillas-Gonzalez, J.; Virgili, T.; Gambetta, A.; Lanzani, G.; Anthopoulos, T. D.; De Leeuw, D. M. *Phys. Rev. Lett.* **2006**, *96*, 106601.

(21) Pranculis, V.; Infahsaeng, Y.; Tang, Z.; Devižis, A.; Vithanage, D. A.; Ponseca, C. S.; Inganäs, O., Jr.; Yartsev, A. P.; Gulbinas, V.; Sundström, V. *J. Am. Chem. Soc.* **2014**, *136*, 11331−11338.

(22) Jenatsch, S.; Hany, R.; Véron, A. C.; Neukom, M.; Züfle, S.; Borgschulte, A.; Ruhstaller, B.; Nüesch, F. *J. Phys. Chem. C* **2014**, *118*, 17036−17045.

(23) Wicht, G.; Bücheler, S.; Dietrich, M.; Jäger, T.; Nüesch, F.; Offermans, T.; Tisserant, J.-N.; Wang, L.; Zhang, H.; Hany, R. *Sol. Energy Mater. Sol. Cells* **2013**, *117*, 585−591.

(24) Jenatsch, S.; Geiger, T.; Heier, J.; Kirsch, C.; Nüesch, F.; Paracchino, A.; Rentsch, D.; Ruhstaller, B.; Véron, A. C.; Hany, R. *Sci. Technol. Adv. Mater.* **2015**, *16*, 035003.

(25) Devižis, A.; Hertel, D.; Meerholz, K.; Gulbinas, V.; Moser, J.-E. *Org. Electron.* **2014**, *15*, 3729−3734.

(26) Drori, T.; Sheng, C. X.; Ndobe, A.; Singh, S.; Holt, J.; Vardeny, Z. V. *Phys. Rev. Lett.* **2008**, *101*, 037401.

(27) Jeglinski, S.; Vardeny, Z. V.; Moses, D.; Srdanov, V. I.; Wudl, F. *Synth. Met.* **1992**, *50*, 557−563.

(28) Kazaoui, S.; Minami, N.; Tanabe, Y.; Byrne, H. J.; Eilmes, A.; Petelenz, P. *Phys. Rev. B* **1998**, *58*, 7689.

(29) Pivrikas, A.; Sariciftci, N. S.; Juška, G.; Österbacka, R. *Prog. Photovoltaics: Res. Appl.* **2007**, *15*, 677−696.

(30) Frankevich, E.; Maruyama, Y.; Ogata, H. *Chem. Phys. Lett.* **1993**, *214*, 39−44.

(31) Frankevich, E. L.; Maruyama, Y. *ICSM'94, Int. Conf. Sci. Technol. Synth. Met.* **1994**, 425−425.

(32) Haddon, R. C.; Perel, A. S.; Morris, R. C.; Palstra, T. T. M.; Hebard, A. F.; Fleming, R. M. *Appl. Phys. Lett.* **1995**, *67*, 121−123.

(33) Kobayashi, S.; Takenobu, T.; Mori, S.; Fujiwara, A.; Iwasa, Y. *Sci. Technol. Adv. Mater.* **2003**, *4*, 371−375.

(34) Burkhard, G. F.; Hoke, E. T.; Beiley, Z. M.; McGehee, M. D. *J. Phys. Chem. C* **2012**, *116*, 26674−26678.

(35) Hedley, G. J.; Ward, A. J.; Alekseev, A.; Howells, C. T.; Martins, E. R.; Serrano, L. A.; Cooke, G.; Ruseckas, A.; Samuel, I. D. *Nat. Commun.* **2013**, *4*, 2867.

(36) Ebbesen, T. W.; Tanigaki, K.; Kuroshima, S. *Chem. Phys. Lett.* **1991**, *181*, 501−504.

(37) Gevaert, M.; Kamat, P. V. *J. Phys. Chem.* **1992**, *96*, 9883−9888.

(38) Sauve, G.; Dimitrijevic, N. M.; Kamat, P. V. *J. Phys. Chem.* **1995**, *99*, 1199−1203.

(39) Vandewal, K.; Albrecht, S.; Hoke, E. T.; Graham, K. R.; Widmer, J.; Douglas, J. D.; Schubert, M.; Mateker, W. R.; Bloking, J. T.; Burkhard, G. F.; Sellinger, A.; Fréchet, J. M. J.; Amassian, A.; Riede, M. K.; McGehee, M. D.; Neher, D.; Salleo, A. *Nat. Mater.* **2014**, *13*, 63−68.

(40) Ruoff, R. S.; Tse, D. S.; Malhotra, R.; Lorents, D. C. *J. Phys. Chem.* **1993**, *97*, 3379−3383.